

Power density spectrum of NGC 5548 and the nature of its variability

B. Czerny¹, A. Schwarzenberg-Czerny^{1,2}, and Z. Loska¹

¹*N. Copernicus Astronomical Center, Bartycka 18, 00-716 Warsaw, Poland*

²*Astronomical Observatory of Adam Mickiewicz University, ul. Słoneczna 36, 60-286 Poznan, Poland*

13 June 2021

ABSTRACT

We derive power density spectra in the optical and X-ray band in the timescale range from several years down to \sim a day. We suggest that the optical power density spectrum consists of two separate components: long timescale variations and short timescale variations, with the dividing timescale around 100 days. The shape of the short timescale component is similar to X-ray power density spectrum which is consistent with the interpretation of short timescale optical variations being caused by X-ray reprocessing. We show that the observed optical long timescale variability is consistent with thermal pulsations of the accretion disc.

Key words: galaxies: active – galaxies:individual:NGC5548 – instabilities – X-rays:galaxies.

1 INTRODUCTION

Systematic multiwavelength study of radio quiet Active Galactic Nuclei (AGN) led to the emergence of the general picture of such a nucleus as a massive black hole surrounded by a relatively cool accretion disc of an outer radius below ~ 1 pc and a hot optically thin plasma (see Mushotzky, Done & Pounds 1993). Comptonization of the soft photons by the plasma leads to emergence of strong X-ray emission from the nucleus.

This compact unresolved region is surrounded by a dusty torus (see Antonucci 1993), marginally resolved in the IR at the distance scales below 100 pc in the case of the nearest AGN (see e.g. Greenhill et al. 1996 for water maser emission from NGC 1068) although not in the case of NGC 5548.

The models of the compact innermost region have to reproduce the results of the detailed studies of the spectra of Seyfert 1 galaxies. X-ray observations were particularly successful in demonstrating the coexistence of the hot and cold gas close to the black hole through the detection of the reflection component (Pounds et al. 1990) and subsequent identification of the observed 6.4 keV iron line profile in a number of sources with the reflection from relativistic accretion disc (Mushotzky et al. 1995 for IC 4329A and NGC 5548, Tanaka et al. (1995) for MCG-6-30-15, Yaqoob et al. 1995 for NGC 4151, Yaqoob et al. 1996 for NGC 7314, Nandra et al. 1997a for NGC 3516 and Weaver et al. 1997 for MCG -5-23-16; for a general discussion see Nandra et al. 1997b).

The shape of the high frequency tail of the X-ray spectra

shows that the velocity distribution of electrons in the hot plasma is predominantly thermal (e.g. Gondek et al. 1996 and Zdziarski et al. 1997 for averaged Seyfert 1 spectra, and Zdziarski, Johnson & Magdziarz 1996 for NGC 4151).

However, the dynamics of this multi-phase medium feeding the black hole is still not understood although a number of attempts to construct a complete - usually stationary - model were undertaken (e.g. Narayan, McClintock & Yi 1996, Witt, Czerny & Życki 1997). The best way to learn which processes might dominate the flow is to study the variability of the nucleus since the variations can be directly related to dynamics whilst the spectra may be insensitive to dynamical parameters.

Extensive studies of variability were done so far mostly for galactic X-ray sources, including black holes. In the case of AGN, most of the studies were constrained to the observations of the spectral changes based on a few spectra and to the studies of the time delays between different spectral bands. Nevertheless those studies of a few monitored AGN brought important conclusions: the well correlated variability in the optical, UV, EUV and X-ray band and the lack of measurable delay between those frequency bands suggested that the optical/UV variability is caused by the reprocessing of the variable X-ray flux (e.g. Collin-Souffrin 1991, Clavel et al. 1992).

However, detailed studies of that hypothesis were difficult. Power spectra were constructed only for the X-ray data and early results based on long EXOSAT lightcurves showed that the PDS was a featureless power law without any characteristic timescale (McHardy & Czerny 1987 for NGC 5506, Lawrence et al. 1987 for NGC 4051).

The situation is changing during the last years. Due to the undertaken monitoring of several AGN more and more data in different wavebands are available. It is therefore important to study the physical constraints to the models imposed by these data.

It is also important to compare the results of variability studies for AGN to what we know about the variability of galactic black holes. The question is the possibility of scaling of some, or most, properties of the flow with the mass of the black hole which may extend over orders of magnitudes, from 10^{10} of solar masses down to ten. If such a scaling exists for some properties, the difference in the timescales of the AGN and galactic black holes help to study them in a complementary ways. Long evolution is easier to study for galactic sources, as the timescales of years for galactic sources correspond to millions of years for AGN. On the other hand the timescales shorter than the travel time through the horizon of a black hole, of order of tens or hundreds of seconds for AGN and of orders of tens of microseconds for a galactic black holes are easier to reach for AGN.

In this paper we derive the power density spectrum of NGC 5548 in the optical band based on the data presented by Sergeev et al. (1997) including the data collected by AGN Watch team. We extend the PDS towards high frequencies using the nonlinear prediction method. We estimate the broad timescale PDS in X-ray band and we compare it to the optical one. We compare these distributions to the present knowledge of other AGN and of galactic X-ray sources. Finally, we discuss the physical mechanisms of the observed optical variations.

2 THE OBSERVATIONAL DATA FOR NGC 5548

The nearby Seyfert galaxy NGC 5548 ($z=0.0174$) is the most extensively observed AGN. The optical/UV variability of this object was followed systematically by International AGN Watch (Peterson et al. 1991; Peterson et al. 1992; Peterson et al. 1994; Korista et al. 1995) during the last five years. The X-ray variability was recently studied by Nandra & Pounds (1994) and Clavel et al. (1992) in the hard X-rays, by Done et al. (1995) in soft X-ray band, and new results are expected from XTE. The EUVE variability was detected by Marshall, Fruscione & Carone (1995) (see also Marshall et al. 1997). These data allowed to formulate first phenomenological models of the time behaviour of the flow in this object (e.g. Rokaki, Collin-Souffrin & Magnan 1993; Loska & Czerny 1997; Magdziarz et al. 1997).

2.1 Optical data

In this paper we use the data obtained by AGN Watch team (Peterson et al. 1994) together with data accumulated over the past ten years prior to the AGN Watch activity and made recently publicly available (Sergeev et al. 1997).

The entire optical data set covers the period from 1977 to 1993. Although the calibration of the data may not be very accurate (see Sergeev et al. 1997) the amplitude of the variability is large (close to factor 3) and small calibration errors of order of 3 percent cannot influence the general picture.

Basic properties of this lightcurve become apparent by simple visual inspection. The variations cover all timescales but the amplitude of variations is related to the timescale. In the shortest timescales, day-to-day changes do not exceed several percent. Within one year, large variations of order of 40 percent peak-to-peak occurred. However, the lightcurve appears flat over the whole interval of 17 years, indicating possible deficit of fluctuations with longest time scales exceeding several years.

2.2 X-ray data

The X-ray power density spectrum was already obtained by Papadakis & Lawrence (1993). It was derived only on the basis of relatively short observations made by EXOSAT satellite which covered only timescales below 0.3 d (more precisely, between 3×10^4 and 5×10^2 s), beyond the range covered by the optical data. The PDS was best described as a power law with additional QPO type feature at $\sim 10^3$ s. The slope of the aperiodic variability was not determined accurately even for the longest data set from July 1984 ($\alpha = 1.99 \pm 0.9$). The variations in the 2-10 keV flux in this EXOSAT data of the length of 1.006 d reach the value 0.42×10^{-11} erg/s/cm² (Kaastra & Barr 1989).

We will try to estimate the X-ray PDS at longer timescales using the following information about the characteristic variability amplitudes.

The variations observed by Ginga during the 42 days of monitoring reached the amplitude 1.58×10^{-11} erg/s/cm² (Clavel et al. 1992). The strong brightening of the source in the optical band in 1984 was accompanied by only a moderate brightening in X-rays showing that the amplitude of variations in timescales of ~ 6 years increases only up to 1.73×10^{-11} erg/s/cm².

3 RESULTS

3.1 The optical power density spectrum for NGC 5548

We study the optical lightcurve of NGC 5548 using the Fourier analysis method. Although a number of other techniques were applied to study variability, determination of the power density spectrum still remains the basic approach even in the study of aperiodic variability (e.g. van der Klis 1995).

In the case of AGN only X-ray (and not the optical) variability was studied in such way, with exception of a BL Lac object OJ 287 (Silanpää et al. 1996), since the time extension and the coverage by optical data is usually not good enough to perform that kind of analysis.

We calculate the power density spectrum (PDS) using an algorithm of Deeming (1975) and applying sufficient sampling interval of $0.00001 d^{-1}$. In order to reduce the noise and to enhance the signal we smooth the power spectrum with a median filter and then bin it on the log scale. Following Korista et al. (1995) we adopt such normalization, that PDS is computed in units of flux squared times day, i.e. $10^{-30} (erg/cm^2 s \text{Å})^2 d$. At redshift $z = 0.0174$ the adopted unit of PDS corresponds to power in B band of $30 \times 10^{18} L_{B\odot}^2 d$ (c.f. Korista et al., 1995). No correction for

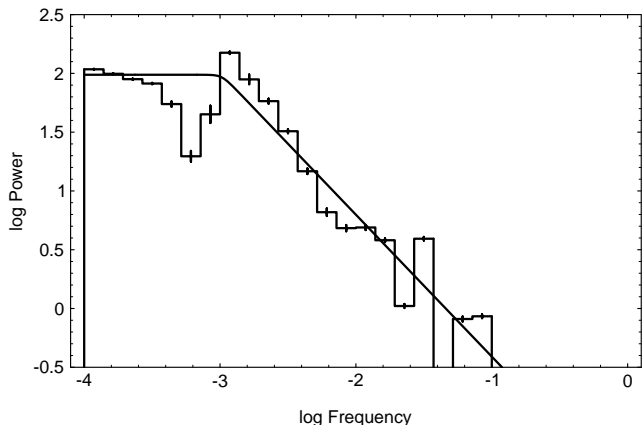


Figure 1. The smoothed and binned power density spectrum of NGC 5548 in the optical band plotted in the decimal log-log scales. On the horizontal axis frequency is in units of cycles per day. On the vertical axis power density is in units of $10^{-30}(\text{erg}/\text{cm}^2\text{s}\text{\AA})^2\text{d}$. Continuous line is a broken power law fit to the power spectrum, with the slope 1.17.

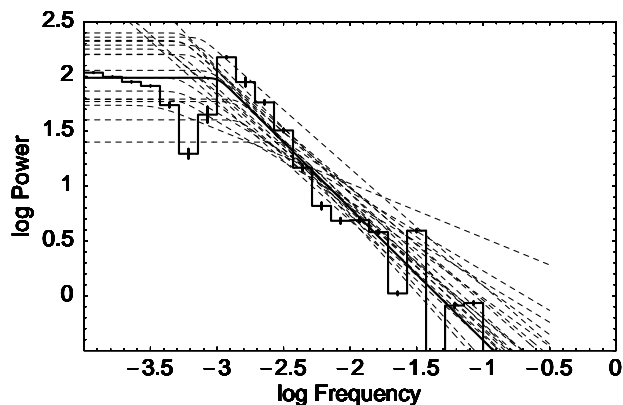


Figure 2. The smoothed and binned power density spectrum of NGC 5548 given as in Fig. 1, together with a direct fit (continuous line). Dashed lines show examples of numerical simulations probing the influence of the window function onto the fit.

power leaks to high frequency induced by window function was applied. Simulations demonstrate that leaks are critical for spectral indices approaching -2 (Green, McHardy & Lehto 1993). Major source of uncertainty in our power spectrum are low frequency fluctuations for which statistics in our data is poor and which contribute large fraction of total power in the power spectrum.

The resulting PDS is shown in Fig. 1. It is plotted in log-log axis usually adopted in X-ray variability analysis. Timescales shorter than ~ 30 days are dominated by white noise and better time resolution is required to study that range. We subtracted this constant component from the whole spectrum before plotting. The overall spectrum is

dominated by clearly aperiodic signal. It can be described as a power law with index $\sim -1.17 \pm 0.04$ flattening off at time scales longer than about 3 years. We show the fit of such a power density shape to the observed one (Fig.1, continuous line).

The above error estimates base on the internal scattering of the residuals from the fit. The influence of the window function itself on the shape of the spectrum was analysed by Papadakis & Lawrence (1995). They conclude that the power leak to high frequencies is negligible for inclinations flatter than -2. Our own extensive simulations (Schwarzenberg-Czerny et al, in preparation) show that the actual external error of the slope may be as large as 0.2. However, the simulations confirm the existence of the break - its frequency is reproduced with accuracy $\log\nu_o = 3.2 \pm 0.3$. Exemplary results of such simulations are shown in Fig. 2.

At lowest frequencies our PDS is affected by smoothing. Hence we performed independent analysis of low-frequency variations. For this purpose we splitted data into two parts, namely AGN Watch data and pre-Watch data and then computed moments for each part separately. Variances in two parts are identical, corresponding to standard deviation of individual observation of $\sigma = 1.63$. Corresponding averages, namely 8.61 and 10.05 differ by less than a standard deviation. This may mean that PDS at lowest frequencies does not exceed average PDS value, in agreement with Fig.1. Note that because of correlation of individual observations, we expect difference of averages considerably in excess of white noise expectation $\sigma/\sqrt{(n-1)}$. This argument, as model independent, is stronger than any results from the simulations. Our simulations, however, support this conclusion (Schwarzenberg-Czerny et al, in preparation).

Therefore, the flattening of the optical PDS at low frequencies is a real property of the data. However, we cannot tell from this analysis whether actually the change of slope is rapid, or gradual. The results of the nonlinear prediction method seem to support the second possibility (see Section 3.2).

Formally, our PDS indicates the presence of a periodicity, or quasi-periodicity, at a knee of the basic shape (i.e. ~ 2.5 years), and its harmonics of 1.2 years. These features are still better seen before smoothing and binning of the PDS. However, the significance of that feature is doubtful for several reasons. On the one hand, the whole data cover only 7 periods for such a timescale. The power at this time scale comes from the two minima observed in 1990 and 1992 as the PDS computed for data excluding this minima does not display this feature. Any process generating large fluctuations would produce such PDS features if by chance exactly two of them occurred during the observed interval. Let us assume for the moment that the probability of observing minima in the lightcurve of NGC5548 is uniform in time. Then, the probability of finding two of them within 2.5 years during the 17 years of observations is as high as $2.5/17 \sim 0.15$.

3.2 The results of the nonlinear prediction method for NGC 5548

The high frequency behaviour of the data is better analysed with the use of the nonlinear prediction method which is sensitive to the timescales as short as the typical separa-

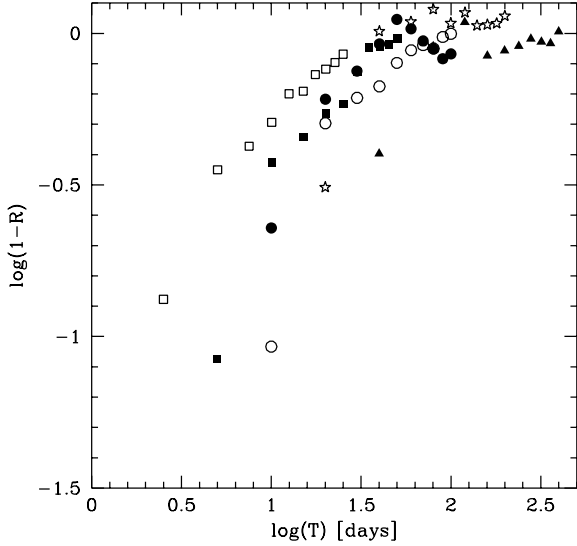


Figure 3. The quality of prediction as a function of the prediction time-step for different timestep of the interpolated data: open squares (2.5 d, AGN Watch data), filled squares (5 d, AGN Watch data), open circles (10 d, AGN Watch), filled circles (10 d, whole data), stars (20 d, whole data), filled triangles (40 d, whole data)

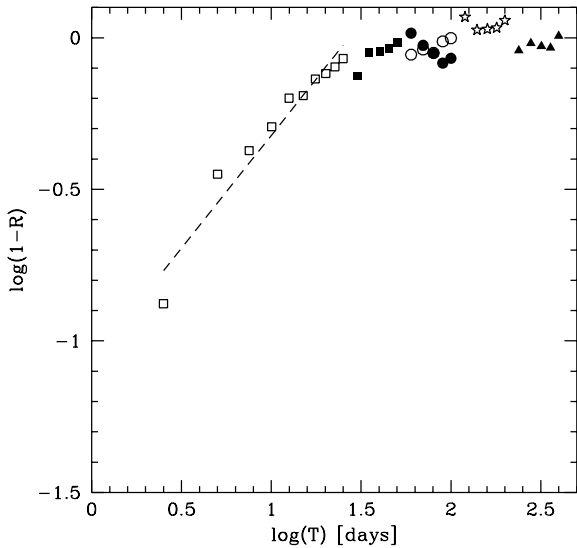


Figure 4. The quality of prediction as a function of the prediction time-step: the combined picture. Data for prediction time below 25 d are from interpolation 2.5 d set, between 20 d and 50 d from interpolation 5 d set, from 50 d to 100 d from interpolation 10 d set (for AGN Watch data and, separately, from whole data), between 100 d and 200 d from interpolation 20 d set and finally between 200 and 400 d from interpolation 40 d set. The correlations for the longest prediction time steps are close to zero. The dashed line shows the linear fit to the high frequency part well approximated by a power law. The slope of this power law equal to 0.74 corresponds to the PDS slope 1.74.

tion between the measurements. This method, introduced by Tsonis & Elsner (1992) and successfully applied to X-ray data for AGN by Czerny & Lehto (1997) is based on the quantitative analysis of the decay of the correlation between any two short sequences in the data with an increase of the time separation of those sequences. It does not require any subtraction of the white noise.

The correlation coefficient R is usually a decreasing function of the time separation T . If the signal is well represented by a simple shot noise, its PDS is well described by a power law with an index α and at the same time the functional form of the dependence $R(T)$ takes the shape

$$1 - R(T) \propto T^{\alpha-1}. \quad (1)$$

Therefore, in the case of non-periodic signal with basically a power law shape of PDS the nonlinear prediction method can be used to determine independently the slope of the PDS.

The method was developed for the equally spaced data with gaps so the original data had to be interpolated.

To study the shortest timescales we used the data collected by AGN Watch team. The mean separation of the data points is 3.4 days, with sequences sampled as densely as 1 day during the fifth year so we adopted the timestep 2.5 d for interpolation. We included only these data points which were interpolated between the original data points separated not more than 1.6 times the adopted timestep.

The resulting correlation coefficient R between the actual and predicted values of the flux as a function of the prediction time T is shown in Fig. 3 (open squares). The $\log(1-R)$ vs. $\log(T)$ plot is generally of a power law shape although a conclusion about the presence of some curvature cannot be rejected. The slope of this power law is equal 0.74 which translates into the slope of the PDS equal 1.74 between the frequencies 0.04 and 0.4 d^{-1} .

The signal is clearly of stochastic nature and not of deterministic chaos since the linear fit to $\log(1-R)$ vs. $\log(T)$ is much better (the correlation coefficient equal 0.95) than the linear fit to $\log(1-R)$ vs. T diagram (the correlation coefficient equal 0.83).

We repeated the analysis assuming the interpolation timestep equal 5 and 10 d (filled squares and open circles) which provided results for longer timescales. The slopes do not differ more than by 0.1 from the previous case although for longer timescales the slope is determined with larger error. Also the statistics of the pairs for prediction becomes a problem. Therefore we repeated the analysis for 10 d interpolation timestep using the whole data, i.e. including the entire period of 17 years of observations (Fig. 3, filled circles). We also attempted to detect the long timescale trends using 20 d and 40 d interpolation timestep but these results are already very close to $R=0$ line (no correlation).

In all computations the dimension of the string d (i.e. the length of the data sequence used for prediction; see Czerny & Lehto 1997) was obtained from the criterion that the correlation for prediction over a single timestep is the largest. In all cases d was equal 1.

As the best representation of the data we choose the results obtained from 2.5 d interpolation step, supplemented at longer timescales by the computations made with the use of consecutive longer interpolation timesteps (Fig. 4). However, it is difficult to make any definite statement about

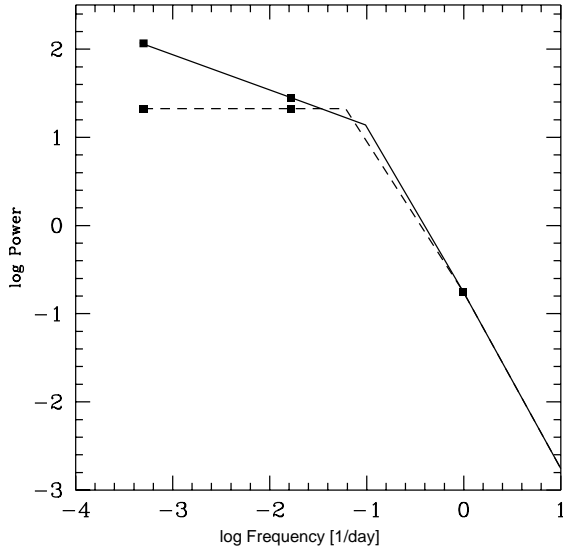


Figure 5. The X-ray power density spectrum in 2 - 10 keV in units $10^{-22}(\text{erg}/\text{cm}^2/\text{s})^2\text{d}$. The dashed line shows the solution with adopted low frequency slope equal zero and continuous line shows the solution with the steepest possible slope in low frequency band (see Section 3.3). Points mark the frequencies at which the amplitude was measured.

the flattening of the curve at timescales about 30 d since the correlations at those timescales become very weak.

To see better the comparison between the results based on nonlinear prediction method and on classical Fourier analysis we replot both on a single plot using the proportionality:

$$PDS \propto (1 - R(T))T \quad (2)$$

and adjusting the normalisation to the Fourier results (Fig. 6). The overlapping region is large enough to see that the results of the nonlinear prediction method extend nicely the Fourier derived PDS to high frequencies without any sudden change of the slope. However, a better data would be necessary in order to see whether a step like feature at ~ 50 days is present in the optical data or rather the PDS is well represented by a single component with a significant curvature. Further work of AGN Watch team may resolve this problem.

3.3 X-ray power density spectrum

In view of lack of a complete X-ray luminosity curve covering all relevant time scales we consider maximum range of variability at a given timescale as more robust measure of variance. Given an estimate of the variance at several time scales, we proceed to estimation of power density function $P(\nu)$ using Parseval equation,

$$\text{Var}(\nu_o) = \int_{\nu_o}^{\infty} P(\nu)d\nu \quad (3)$$

which reduces the problem to the inversion of an integral equation. We defer derivation of Eq. (3) and its inversion to Appendix.

At the shortest timescales (below 0.68 day) we adopt the PDS slope equal 1.99 after Papadakis and Lawrence (1993). We normalize it on the basis of equation (2) using the variability amplitude for the 2-10 keV flux in the EXOSAT data given by Kaastra & Barr (1989).

We assumed that PDS between $\nu = 1\text{d}^{-1}$ and $1/6\text{yr}^{-1}$ may be represented by a broken power law with a break at ν_o . The parameters of the power law are determined by inversion of Eq. (3), or more specifically of its particular form (see Appendix, Eq. 5).

In the first solution we assumed $\alpha_2 = 0$. Our solution yields break frequency $\nu_o = 6.0 \times 10^{-2}\text{d}^{-1}$ and the slope $\alpha_1 = 1.71$ (see Fig. 5, dashed line). The position of the ν_o depends very strongly on the difference between the amplitudes at $\nu = 1/42\text{d}^{-1}$ and $1/6\text{yr}^{-1}$ and the last value is actually given by a single measurement so the derived value should be treated as an estimate of the order of magnitude. We also constructed solutions with arbitrary but nonvanishing value of α_2 . The solutions existed only if α_2 was smaller than 0.41. We show this limiting case in Fig. 5 (continuous line).

We are unable to exclude negative values of α_2 , for our method does not work well for non monotonic PDS.

The two limiting cases for the solutions of the constraints imposed on X-ray PDS well illustrate the overall character of the X-ray variability. Clearly, the PDS cannot be a single power law in the entire studied timescale range. However, we cannot tell whether the turnoff is sharp or rather we deal with a broad band curvature.

4 DISCUSSION

4.1 Character of the optical variability

The optical variability is aperiodic and broad band covering all the available timescales from years down to a day. Present data do not allow to distinguish any QPO phenomena superimposed on the broad component although the traces of some substructure in the PDS seem to show up.

The overall variability is dominated by the timescales around 3 years. The PDS would show it clearly if replotted as power per frequency decade i.e. $\log(\text{Power} \times \text{Frequency})$ versus $\log(\text{Frequency})$ diagram, in analogy to popular representation of the radiation flux as $\log(\text{Flux} \times \text{Frequency})$ vs. $\log(\text{Frequency})$. In such a new plot the flat part of the PDS change into an steeply increasing power law peaking at a turn off point at 3 years (See Fig. 7).

The subsequent part, between the timescales from ~ 3 years down to ~ 100 days looks almost flat since the power law index 1.17 is translated into just 0.17 in the new diagram so the PDS is really broad band. This part ends up possibly with a second peak at timescales of about 30 d.

We also cannot reject the hypothesis that the PDS shows a continuous curvature with a single broad flat part covering the timescale range between $\sim 30\text{d}$ and $\sim 3\text{y}$.

At the shortest timescales (below 30 days) the decrease of the variability amplitude is much faster, with PDS index equal 1.74.

The data may therefore represent a single variability mechanism operating most efficiently between the timescales of 3 years and 30 days.

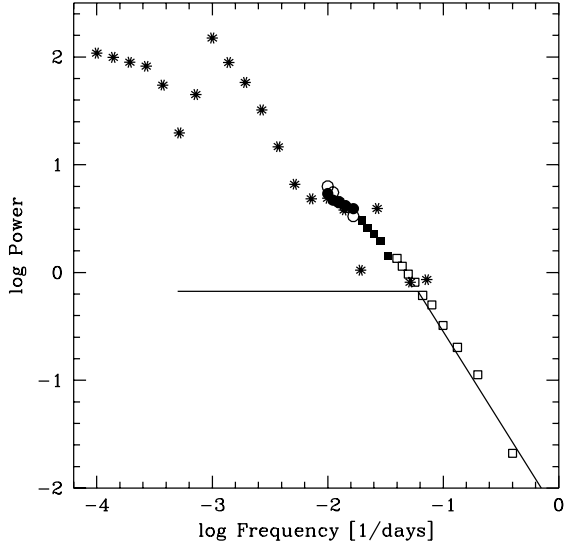


Figure 6. The combined information about the power density spectrum of NGC 5548: stars are the optical PDS from Fig. 1, points of various shape mark the optical PDS derived from the nonlinear prediction method (Fig. 4) for timescales shorter than 100 d, continuous line mark the X-ray PDS from Fig. 5. The normalization of the last two components were adjusted to match the high frequency tail of the first component.

However, a flattening of the PDS at ~ 200 days with subsequent turn off at ~ 30 days may rather suggest that the optical PDS consists of two separate components. The long timescale component has a flat PDS above 3 years and turns down with an index somewhat steeper than the overall 1.17. At the shortest timescales there is an onset of another component which again is flat above 100 days, peaks somewhere at about 30 days and then turns off rather steeply.

4.2 Comparison with X-ray variability of NGC 5548

The dominant timescale in X-rays is somewhere around 17 days, although may be a factor of a few longer if the amplitude at 6 year timescale is underestimated. This is clearly different from the timescale of 3 years dominating the optical variability. However, it coincides interestingly with some substructure present in the optical PDS at the timescale of ~ 100 days.

Particularly, if the optical PDS consists of two components, as suggested in Section 4.1, we can roughly identify the X-ray PDS shape with the short timescale component. In both cases the PDS is flat above 100 days, the turnover is around ~ 30 days (30 in Fourier approach, 30 in nonlinear prediction and 17 in X-ray data) and the slope after the turn-off is steep (-1.71 for the timescales of days in X-rays, -1.74 in optical band).

In order to show better the comparison of the optical and X-ray PDS we placed the X-ray PDS on the same plot as the optical one (see Figs. 6 and 7). Since in that case units are clearly different we adopted the normalization of the X-ray PDS in that case as arbitrary and we adjusted it

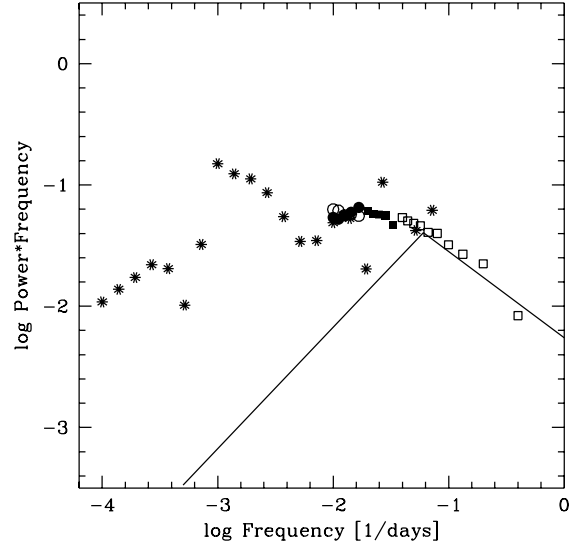


Figure 7. The same as Fig. 6 but after multiplication by the frequency to show the power per logarithmic unit of the frequency; the peak on this diagram shows the frequencies at which most of the power resides.

to the high frequency tail of the optical PDS. The deficit of the power in X-ray PDS with respect to the optical PDS at longer timescales are now clearly seen.

Therefore the data seem to suggest the possibility that on the timescales longer than ~ 100 days the optical variability is unrelated to X-ray variations while on the timescales below ~ 100 days the shape of the optical PDS is dominated by another component of the shape similar to X-ray PDS.

4.3 Comparison with X-ray variability of AGN

X-ray PDS for other AGN are determined more accurately. For us the most interesting cases are two Seyfert galaxies studied in the broad frequency range.

NGC 5506 is a bright Seyfert 2 galaxy. The long history of the X-ray measurements of that source together with a 3 day continuous observation by EXOSAT allowed to determine its PDS in the entire range from ~ 10 years down to 400 s (McHardy 1989). The shape of the PDS is basically that of a power law with index ~ 1.5 , clearly flattening above the timescales of order of ~ 20 days. Its high frequency part between $10^{-5} - 10^{-3}$ Hz was actually better represented as a broken power law changing index from 1.0 to 1.9 towards high frequencies.

The broad band X-ray PDS spectrum of NGC 5548 derived by us is therefore quite similar to NGC 5506. Even the position of the ν_{flat} is similar which may not be surprising since the luminosities of the two objects are comparable.

NGC 4151 is a nearby moderately bright Seyfert 1.5 galaxy frequently observed in X-rays. The broad band PDS for that galaxy also shows clearly the flat part at timescales ~ 100 days and a power law with index ~ 2.1 between 10^3 and 5×10^4 s (Abraham & McHardy 1989; see also Papadakis & McHardy 1995). It is, however, impossible to tell on the basis of that data whether the flattening progresses

continuously towards low frequencies or a well defined knee is present somewhere at the timescale between a day and several days.

Few other AGN were also studied basing on the long EXOSAT lightcurves which allowed to determine accurately the slope of the PDS for timescales between fraction of an hour and a day. Mean index of that slope determined from a sample of a few objects was 1.7 ± 0.5 (Green et al. 1993) or 1.55 ± 0.09 (Papadakis & Lawrence 1993). Studies based on Ginga data (e.g. McHardy 1989) as well as complementary studies of the old EXOSAT lightcurves made using the non-linear prediction method (Czerny & Lehto 1997) showed that power law continues down to the timescales of 200 s. Recent study of the ASCA data for MCG 6-15-30 with the use of excess pair fraction method (Yaqoob et al. 1997) indicate that the power law with an index ~ 1.5 extends actually down to 20 s timescale. However, no significant change in the slope of the power law was noticed.

Certain degree of success in modelling X-ray lightcurves of AGN was achieved using Linear State Space Models employing first order autoregressive process AR[1] for modelling of dynamics (König & Timmer, 1997). This model accommodates flattening of the spectrum both at low and high frequencies.

4.4 Possible mechanisms of optical variability

The optical variability is dominated by the broad band of timescales starting from 3 years and extending down to shorter timescales with only slowly weakening power.

This timescale is too short for typical viscous evolution which requires thousands of years (see e.g. Siemiginowska, Czerny & Kostyunin 1996). Therefore we look for explanation of the observed behaviour amongst the dynamical or thermal timescales.

4.4.1 Dynamical instabilities

The basic dynamical timescale is given by the Keplerian orbital motion. The mass of the black hole in NGC 5548 is most probably within the range 6×10^7 and $1.4 \times 10^8 M_\odot$ (see e.g. Loska & Czerny 1997, Kuraszkiwicz, Loska & Czerny 1997 and the references therein). Therefore, we can adopt the value $10^8 M_\odot$ as representative.

The dynamical timescale is equal 3 years when the distance x (expressed in units of the Schwarzschild radius) is equal

$$x = 1600 M_8^{2/3}. \quad (4)$$

This distance translates into a distance of 16 light days for $10^8 M_\odot$ black hole.

If the disc does not extend beyond that radius and it is clumpy or dynamically pulsating below it then the observed range of timescales is reproduced.

There are no easy arguments why the disc should be truncated at that radius. However, low ionization broad emission lines (LIL), if formed at the disc surface, (e.g. Collin-Souffrin 1987) show the typical delay of 18 days (Peterson et al. 1994), i.e. about the required light travel time. Also the characteristic timescale for the X-ray variability and the short timescale optical component peaks somewhere

around this value which may correspond to the light travel time across the hot plasma region but those two timescales can be also related in a natural way without any reference to the dynamical timescale in the disc (see Section 4.6).

4.4.2 Thermal instabilities

The thermal timescale at any given radius depends on the assumptions about the properties of an accretion disc. If we assume that the disc structure is well represented by the classical model of Shakura & Sunyaev (1973) then the thermal timescale is longer than the dynamical timescale by a factor α^{-1} , where α is the viscosity parameter. The location of the radius where the thermal timescale is equal to 3 years depends on the adopted value of the viscosity parameter.

The only value suggested for that particular object is 0.03 derived on the basis of the overall optical/UV/X-ray spectra (Kuraszkiwicz et al. 1997) within the frame of the accreting corona model. Adopting that value for a scaling we obtain the radius

$$x = 160 \alpha_{0.03}^{2/3} M_8^{2/3} \quad (5)$$

which is at the distance of 1.6 light day from the central black hole of the mass $10^8 M_\odot$.

The inner parts of AGN accretion discs, within a frame of the α times the total pressure viscosity model, are thermally unstable. We can compare the radius given by equation 4 with the radius where there is the onset of the instability.

Simple estimate of the transition radius from the radiation pressure to gas pressure domination gives (Shakura & Sunyaev 1973)

$$x_{ab} = 46 \alpha_{0.03}^{2/21} M_8^{-2/3} \dot{M}_{0.025}^{16/21} \quad (6)$$

where we adopted the mean accretion rate $0.025 \dot{M}_\odot/\text{yr}$ (after Kuraszkiwicz et al. 1997) as a scaling factor.

This value only weakly depends on the viscosity and is by a factor ~ 3 smaller than expected observationally. However, more accurate computations are encouraging.

Our accretion disc model was computed taking into account the vertical structure of the disc (Róžańska et al. 1998). Free-free opacity was replaced by the appropriate full opacities (Kramers means) in the radiation transfer equation.

The disc is thermally (and viscously) unstable when the ratio β of the gas pressure to the total pressure is smaller than $2/5$ (Shakura & Sunyaev 1976). Since we now compute the vertical structure (so the gas to the total pressure ratio is also a function of the distance from the equatorial plane) we estimate the tendency of the disc to develop the thermal instability by computing, at any radius, the ratio of the disc mass where β is smaller than $2/5$ to the total mass.

In Fig. 8 we show the plot of the fraction of the disc mass which is thermally unstable at a given radius. It is calculated as a ratio of the surface density of the gas with β smaller than $2/5$ to the total surface density.

We see that the instability starts to be present at $\sim 200 R_{Schw}$ and at $150 R_{Schw}$ the entire disc become thermally unstable so the thermal instability of an α disc is a viable explanation of the shape of the long timescale optical PDS.

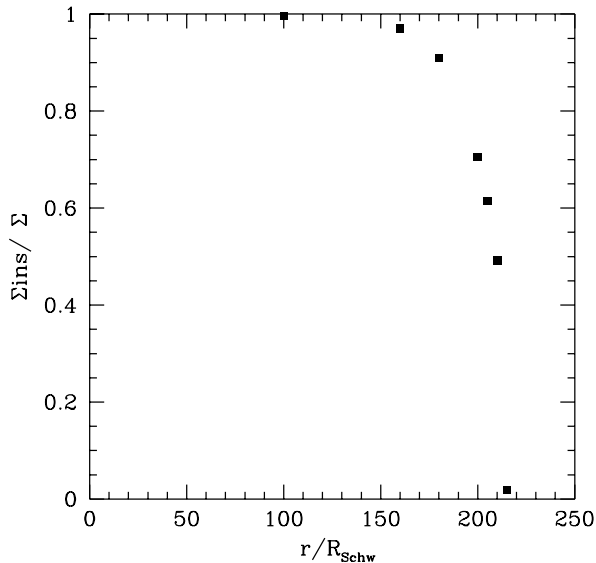


Figure 8. The fraction of the disc which is thermally unstable plotted as a function of radius. Model parameters: $M = 10^8 M_{\odot}$, $\dot{M} = 0.025 M_{\odot}/\text{yr}$ and $\alpha = 0.033$.

4.5 Possible mechanisms of X-ray variability

The interesting conclusions about the nature of X-ray variability were derived so far only for galactic sources. Recent XTE observations of Cyg X-1 (Cui et al. 1997) applied to the concept of coherence function (Vaughan & Novak 1997) suggested that most of the time the hot medium itself is not strongly variable. The observed variability may be caused instead by scattering of the soft photons emitted close to the black hole by an extended medium (Kazanas, Hua & Titarchuk 1997). In this picture the timescale of the flattening of the PDS measures directly the size of the comptonizing region.

In the case of NGC 5548 it would mean that the hot medium extends up to ~ 30 light days.

One of the possibilities is that the Compton heated corona forms above an accretion disc (Begelman, McKee & Shields 1983). The outer radius of such a corona is located at $\sim 10000 R_{\text{Schw}}$ (i.e. 100 light days). The corona, however, scatters photons efficiently only up to $\sim 10\%$ of that distance (e.g. Ostriker, McKee & Klein 1991) which clearly makes an interesting explanation of the presence of the hot medium within the distance required by the shape of the X-ray PDS although it would be necessary to invoke some extra heating in excess of the Inverse Compton temperature.

The fact that the representative emission radius of the H_{β} is comparable to the disc fraction covered by a corona may not be accidental as the presence of the corona scattering the photons emitted closer to the black hole and redirecting a part of them towards the disc surface enhances the emission of lines (see e.g. Kurpiewski, Kuraszewicz & Czerny 1997).

4.6 Comparison with galactic X-ray sources

Rapid aperiodic variability occurs in all types of X-ray binaries (for a review see van der Klis 1995). Since the observed X-ray flux from these objects is typically a few orders of magnitude higher than the observed X-ray flux from AGN the shape of the PDS for galactic sources could have been studied in much more detail than for AGN. Therefore, in order to make an adequate comparison we have to concentrate only on the basic characteristics of galactic sources.

The broad band PDS component consisting of a flat part below the frequency ν_{flat} and a power law with index higher than 1.0 above it is characteristic for several different types of objects in different states.

Black holes clearly display that kind of variability in their low (hard) states, with Cyg X-1 being the best example. The value of ν_{flat} is somewhere around 0.1 Hz but it may vary by a factor of a few between separate observations (Belloni & Hasinger 1990). The power law part index is ~ 1.1 between ν_{flat} and ~ 3 Hz, and it ~ 2.0 at high frequencies. The value of ν_{flat} is 10^7 times higher than the ν_{flat} of the optical PDS for NGC 5548, as it would be expected from a simple scaling with the mass of the central black hole. This fact, together with the slope of the PDS suggests that the X-ray PDS for Cyg X-1 in low state corresponds to the optical (and not X-ray!) PDS for NGC 5548. Similar effect can be present in the case of NGC 4151: X-ray PDS break at 14 d (Lawrence & McHardy 1995) is an order of magnitude too low to provide a perfect analogy with Cyg X-1. Unfortunately, optical PDS is not available for this source.

What is more, the frequency of the change in the PDS slope of Cyg X-1 is again by a factor 10^7 higher than ν_{flat} of the X-ray PDS of NGC 5548 thus indicating again a kind of substructure. Such a view is confirmed by recent high quality XTE observations of that source during the transition from the hard state to the soft state (Cui et al. 1997). In this case the power spectrum is clearly two component, with one component having ν_{flat} at 3 Hz (their Figs. 2 and 3) followed by a steep power law and second component, an underlying power law, relatively flat and without any clear flattening within the studied range of timescales (above 0.03 Hz).

If the explanation of the shape of the optical and X-ray power density spectrum of NGC 5548 is correct (see Section 4.4 and 4.5) we would expect the simple scaling with mass of the central black hole in the case of ν_{flat} from X-ray PDS related to the size of the hot medium. The timescales related to accretion disc also scales roughly with the mass of the central black hole but they are at the same time considerably influenced by the luminosity to the Eddington luminosity ratio.

The question, however, remains why the PDS of galactic Black Hole are similar to optical instead of an X-ray PDS of NGC 5548. In the soft X-ray range the answer may lie in the contamination of the spectrum by the direct contribution of the disc to the X-ray emission due to much higher temperatures of GBH discs due to the scaling as $M^{-1/4}$ with the mass of the black hole. However, in the case of hard X-rays the explanation should be different. It may be related to the fact that viscous timescales are relatively much shorter in galactic objects than in AGN. Therefore, in GBH both timescales can mix since the viscous timescale is only tens

or hundreds times longer than thermal timescales. In AGN the viscous timescales are up to hundreds of thousands times longer than thermal timescales. From that point of view, the observational determination of ν_{flat} in all states is crucial.

The same basic component also dominates the PDS of the island sources - low luminosity accreting neutron stars with negligible magnetic field (see van der Klis 1995). The value of ν_{flat} is in that case ~ 0.3 Hz, again as it would be expected from the scaling of the optical PDS of NGC 5548. It indicates that this kind of variability is not necessarily characteristic only for accreting black holes.

Finally, similar component is also typical for disk-fed X-ray pulsars like Cen X-1, with the value of ν_{flat} again ~ 0.3 Hz.

However, in their high (soft) states black holes are characterized by a single power law PDS shape over several decades, with an index quite close to 1, as in the case of the optical PDS of NGC 5548 at intermediate frequencies. If any flattening is present it has to take place at frequencies lower than 0.001 Hz, at least in some sources. It may be too long for thermal timescales within the thermally unstable part of the disc.

The qualitative changes are characteristic not only for black holes. Also accreting neutron stars change their variability (and spectral) appearance with an increase of the accretion rate. Island sources change into banana sources and the PDS of upper banana sources - a single broad band power law with index only slightly larger than 1 - strongly resemble the soft state of Cyg X-1 (van der Klis 1995).

At this stage our comparison of variability of NGC 5548 with galactic sources indicates both some similarities as well as differences and cannot be conclusive.

5 CONCLUSIONS

Presented results support the view that there are two clearly distinct physical mechanisms responsible for variability of NGC 5548.

In the short timescales (below ~ 100 days) the variability is caused by the Comptonization of the soft photons (emitted by the innermost part of accretion disc, i.e. very close to the black hole) by an extended hot medium, perhaps a corona. This scattering results both in variable X-ray flux and in variable optical flux due to absorption of a fraction of the X-ray flux by the accretion disc. The size of the hot gas region required by the shape of the power density spectrum is well estimated by the theory of the Compton heated corona.

In the long timescales (above ~ 100 days) the optical variability is unrelated to X-rays. It is caused by thermal pulsations of the accretion disc. The size of the region of the disc, required by the shape of the power density spectrum, is consistent with the region dominated by the radiation pressure and therefore thermally unstable within the frame of a standard disc model of Shakura & Sunyaev (1973).

The scaling properties of the variability with mass are difficult to confirm on a basis of a simple comparison of NGC 5548 with the galactic sources. The difficulties lie in the relative closeness of the viscous and thermal timescale in galactic sources (factor 0.01 instead of 0.00001 in AGN) and the contamination of X-rays in galactic sources by a direct

emission of an accretion disc due to the systematic difference in the disc temperatures between AGN and GBH by two orders of magnitude. More research should be done on even approximate extension of the X-ray PDS of other AGN onto the timescales of years and on studies of the shape of PDS of different galactic sources on the timescales longer than 100 s in order to confirm or reject the presented physical interpretations of the variability.

ACKNOWLEDGEMENTS

We thank Andrzej Zdziarski for suggestion to introduce the Power*Frequency plot (Fig. 7) and to the referee, Ian McHardy, for helpful remarks which allowed to improve the manuscript. This work was supported in part by grants 2P03D 004 10 (BCz & ZL) and 2P03D 003 13 (ASC) of the Polish State Committee for Scientific Research (KBN).

REFERENCES

- Abraham, R.G., McHardy, I.M., 1989, in 23rd ESLAB Symposium on Two topics in X-ray Astronomy: 2. AGN and the X-ray Background, ESA-SP 292, page 865
- Antonucci, R.R.J., 1993, ARA&A, 31, 473
- Begelman, M.C., McKee, C.F., Shields, G.A., 1983, ApJ, 271, 70
- Belloni, T., Hasinger, G., 1990, A&A, 227, L33
- Clavel, J. et al., 1992, ApJ, 393, 113
- Collin-Souffrin, S., 1987, A&A, 179, 60
- Collin-Souffrin, S., 1991, A&A, 249, 344
- Cui, W., Zhang, S.N., Focke, W., Swank, J.H., 1997, ApJ, 484, 383
- Czerny, B., Lehto, H.J., 1997, MNRAS, 285, 365
- Deeming, T.J., 1975, ApSS, 36, 137 and an errata.
- Done, C., Pounds, K.A., Nandra, K., Fabian, A.C., 1995, MNRAS, 275, 417
- Gondek, D., Zdziarski, A.A., Johnson, W.N., George, I.M., McNaron-Brown, K., Magdziarz, P., Smith, D., Gruber, D.E., 1996, MNRAS, 282, 646
- Green, A.R., McHardy, I.M. & Lehto, H.J., 1993 MNRAS, 265, 664
- Greenhill, L.J., Gwinn, C.R., Antonucci, R., Barvainis, R., 1996, ApJL, 472, L21
- Kaastra, J.S., Barr, P., 1989, A&A, 226, 59
- Kazanas, D., Hua, X., Titarchuk, L., 1997, ApJ, 480, 735
- Korista, K.T., et al., 1995, ApJS, 97, 285
- König, M. & Timmer, J., 1997, A&AS, 124, 589
- Kuraszkiewicz, J., Loska, Z., Czerny, B., 1997, Acta Astr., 47, 263
- Kurpiewski, A., Kuraszkiewicz, J., Czerny, B., 1997, MNRAS, 285, 725
- Lawrence, A., Pounds, K.A., Watson, M.G., Elvis, M.S., 1987, Nat., 325, 692
- Loska, Z., Czerny, B., 1997, MNRAS, 284, 946
- Magdziarz, P., Blaes, O., Zdziarski, A.A., Johnson, W.N., Smith, D.A., 1997, in Proceedings of the Fourth Compton Symp., eds. C.D. Dermer, J.K. Kurfess and M.S. Strickman (in press)
- Marshall, H.L., Fruscione, A., Carone, T.E., 1995, ApJ, 439, 90
- Marshall, H.L. et al. 1997, ApJ, 479, 222
- McHardy, I.M., Czerny, B., 1987, Nat., 325, 696
- McHardy, I.M., 1989, in 23rd ESLAB Symposium on Two topics in X-ray Astronomy: 2. AGN and the X-ray Background, ESA-SP 292, page 1111
- Mushotzky, R.F., Done, C., Pounds, K.A., 1993, ARA&A, 31, 717

- Mushotzky, R.F., Fabian, A.C., Iwasawa, K., Kunieda, H., Matsumoto, M., Nandra, K., Tanaka, Y., 1995, MNRAS, 272, L9
- Nandra, K., George, I.M., Mushotzky, R.F., Turner, T.J., Yaqoob, T., 1997a, ApJ, 477, 602
- Nandra, K., Mushotzky, R.F., Yaqoob, T., George, I.M., Turner, T.J., 1997b, MNRAS, 284, L7
- Nandra, K., Pounds, K.A., 1994, MNRAS, 268, 405
- Narayan, R., McClintock, J.E., Yi, I., 1996, ApJ, 431, 359
- Ostriker, E.C., McKee, C.F., Klein, R.I., 1991, ApJ, 377, 593
- Papadakis, I., Lawrence, A., 1993, Nat., 361, 233
- Papadakis, I., Lawrence, A., 1995, MNRAS, 272, 161
- Papadakis, I. and McHardy, I.M., 1995, MNRAS, 273, 923-939
- Peterson, B.M. et al., 1991, ApJ, 368, 119
- Peterson, B.M. et al., 1992, ApJ, 392, 470
- Peterson, B.M. et al., 1994, ApJ, 425, 622
- Pounds, K.A., Nandra, K., Steward, G.C., George, I.M., Fabian, A.C., 1990, Nat., 344, 132
- Rokaki, E., Collin-Souffrin, S., Magnan, C., 1993, A&A, 272, 8
- Różańska, A., Czerny, B., Życki, P.T. Pojmański, G., 1998 (submitted to MNRAS)
- Sergeev S.G., Pronik, V.I., Malkov, Yu.F., Chuvaev, K.K., 1997, A&A, 320, 405
- Shakura, N.I., Sunyaev, A.R., 1973, A&A, 24, 337
- Shakura, N.I., Sunyaev, R.A., 1976, MNRAS, 175, 613
- Siemiginowska, A., Czerny, B., Kostyunin, V., 1996, ApJ, 458, 491
- Silanpää, A., et al. 1996, A&A, 305, L17
- Tanaka, Y., et al., 1995, Nat., 375, 659
- Tsonis, A.A., Elsner, J.B., 1992, Nat., 358, 217
- Van der Klis, M., 1995, in X-ray Binaries, eds. W.H.G. Lewin, J. van Paradijs & E.P.J. van den Heuvel, Cambridge University Press, p. 252
- Vaughan, B., Nowak, M., 1997, ApJ, 474, L43
- Weaver, K.A., Yaqoob, T., Mushotzky, R.F., Nousek, J., Hayashi, I., Koyama, K., 1997, ApJ, 474, 675
- Witt, H.J., Czerny, B., Życki, P.T., 1997, MNRAS, 286, 848
- Yaqoob, T., Edelson, R., Weaver, K., Warwick, R.S., Mushotzky, R.F., Serlemitsos, P.J., Holt, S.S., 1995, ApJ, 453, L81
- Yaqoob, T., Serlemitsos, P.J., Turner, T.J., George, I.M., Nandra, K., 1996, ApJ, 470, L27
- Yaqoob, T., McKernan, B., Ptak, A., Nandra, K., Serlemitsos, P.J., 1997, ApJL (in press)
- Zdziarski, A.A., Johnson, W.N., Magdziarz, P., 1996, MNRAS, 283, 193
- Zdziarski, A.A., Johnson, W.N., Poutanen, J., Magdziarz, P., Gierliński, M., 1997, CAMK preprint 316

APPENDIX

Link between variance and power density spectrum (PDS) may be established using Parseval equation:

$$\int_{-\infty}^{\infty} |f(t)|^2 dt = \int_{-\infty}^{\infty} |\mathcal{F}(\nu)|^2 d\nu \quad (1)$$

Let us consider model signal $f(t)$ binned in time intervals δt differing from null in the observed time interval T and vanishing elsewhere. Signal $f(t)$ constitutes an example of a band limited signal. Its Fourier transform decreases outside frequency band $< 1/T, 1/\delta t >$. Taking this into account and assuming reality of f , so that $|\mathcal{F}(-\nu)|^2 = |\mathcal{F}(\nu)|^2$ one obtains approximation of Eq. (1) in the following approximate form

$$\int_{-T/2}^{T/2} |f(t)|^2 dt \approx 2 \int_{1/T}^{1/\delta t} |\mathcal{F}(\nu)|^2 d\nu \quad (2)$$

Without loss of generality we may assume here that mean value was subtracted from data so that $\langle f \rangle = 0$. Then LHS of Eq. (2) reduces to variance estimate $\langle Var(\nu) \rangle$. Modulus of Fourier transform in RHS $|\mathcal{F}(\nu)|^2$ may be expressed by PDS $P(\nu)$, but normalization requires care. We use Deeming (1975) Eq. (61) to ensure proper normalization. We take into account that, for considered δt and shape of PDS, integration up to $1/\delta t$ is equivalent to integration to infinity. Finally we obtain Eq. (3):

$$T \langle Var(\nu) \rangle = 2T \int_{\nu}^{\infty} P(\nu') d\nu' \quad (3)$$

In this paper we consider PDS consisting of two power laws, joined at ν_o :

$$P(\nu) = \begin{cases} P_o (\nu/\nu_o)^{-\alpha_1} & \nu > \nu_o \\ P_o (\nu/\nu_o)^{-\alpha_2} & \nu < \nu_o \end{cases} \quad (4)$$

where P_o , ν_o , α_1 and α_2 are constants. Then integration in Eq. (3) may be carried analytically yielding:

$$\langle Var(\nu) \rangle = \begin{cases} \frac{2P_o\nu_o}{1-\alpha_1} \left(\frac{\nu}{\nu_o}\right)^{1-\alpha_1} & \nu > \nu_o \\ \frac{2P_o\nu_o}{1-\alpha_2} \left(1 - \frac{\nu}{\nu_o}\right)^{1-\alpha_2} + \langle Var(\nu_o) \rangle & \nu < \nu_o \end{cases} \quad (5)$$

Equation (5) may be effectively solved for $P(\nu)$ as long as $\nu P(\nu)$ is monotonically decreasing with ν . X-ray data at hand seem to be consistent with that. We substitute observed X-ray variances into Eq. (5) and solve for parameters α , P_o and ν_o .

This paper has been processed by the authors using the Blackwell Scientific Publications L^AT_EX style file.